The Journal of Immunology

Mechanisms of the Innate Defense Regulator Peptide-1002 Anti-Inflammatory Activity in a Sterile Inflammation Mouse Model

Bing Catherine Wu, Amy Huei-Yi Lee and Robert E. W. Hancock

J Immunol published online 9 October 2017
http://www.jimmunol.org/content/early/2017/10/07/jimmunol.1700985

The Journal of Immunology is published twice each month by
The American Association of Immunologists, Inc.,
1451 Rockville Pike, Suite 650, Rockville, MD 20852

Print ISSN: 0022-1767 Online ISSN: 1550-6606.

Published October 9, 2017, doi:10.4049/jimmunol.1700985

Mechanisms of the Innate Defense Regulator Peptide-1002 Anti-Inflammatory Activity in a Sterile Inflammation Mouse Model

Bing Catherine Wu, Amy Huei-Yi Lee, and Robert E. W. Hancock

Innate defense regulator (IDR) peptide-1002 is a synthetic host defense peptide derivative with strong anti-inflammatory properties. Extending previous data, IDR-1002 suppressed in vitro inflammatory responses in RAW 264.7 murine monocyte/macrophage cells challenged with the TLR4 agonist LPS and TLR2 agonists lipoteichoic acid and zymosan. To investigate the anti-inflammatory mechanisms of IDR-1002 in vivo, the PMA-induced mouse ear inflammation model was used. Topical IDR-1002 treatment successfully dampened PMA-induced ear edema, proinflammatory cytokine production, reactive oxygen and nitrogen species release, and neutrophil recruitment in the ears of CD1 mice. Advanced RNA transcriptomic analysis on the mouse ear transcriptome revealed that IDR-1002 reduced sterile inflammation by suppressing the expression of transmembrane G protein–coupled receptors (class A/1 rhodopsin-like), including receptors for chemokines, PGs, histamine, platelet activating factor, and anaphylatoxin. IDR-1002 also dampened the IFN-γ response and repressed the IFN regulatory factor 8–regulated network that controls central inflammatory pathways. This study demonstrates that IDR-1002 exhibits strong in vitro and in vivo anti-inflammatory activities, informs the underlying anti-inflammatory mechanisms, and reveals its potential as a novel therapeutic for inflammatory diseases. ***The Journal of Immunology*****, 2017, 199: 000–000.**

Inflammation is a vital part of the body's first line of defense. A controlled inflammatory response can protect against foreign invaders, eliminate damaged cells, and initiate tissue repair (1). Inflammatory responses triggered by stimuli from nonmicrobial origins, such as irritants, are termed sterile inflammation (2). Sterile inflammation is characterized by neutrophil and macrophage infiltration and the production of reactive oxygen species (ROS) and proinflammatory cytokines, such as TNF and IL-1 (2–5). Dysregulated and prolonged sterile inflammation underlies the pathogenesis of many human diseases, including Alzheimer's disease, asthma, atherosclerosis, chronic obstructive pulmonary disease, and rheumatoid arthritis (6–10). Despite the availability of different treatment options, there is no cure for many of these inflammatory disorders. Moreover, the use of immune suppression as a common therapeutic strategy can lead to higher risk for infectious diseases (11–13). Therefore, immune modulators that dampen excessive inflammation without compromising appropriate immune responses to infections can serve as superior therapeutic solutions.

Innate defense regulator (IDR) peptides are synthetic immunomodulatory agents derived from evolutionarily conserved host defense peptides (HDPs) (14–17). Under physiological conditions, HDPs and IDRs exhibit a variety of immunomodulatory functions including recruitment of immune cells, modulation of chemokine and cytokine levels, promotion of wound healing, stimulation of angiogenesis, and polarization of macrophage differentiation (14–17). IDR-1002 was initially selected from a library of bactenecin derivatives based on its enhanced ability to induce chemokines from human PBMCs, which correlated with protection against *Staphylococcus aureus* and *Escherichia coli* infections in vivo (18). IDR-1002 was also able to effectively dampen proinflammatory cytokine induction in response to inflammatory agonists in vitro (19–21). Previous research has demonstrated that IDR-1002 can significantly suppress LPS-mediated neutrophil degranulation and the release of ROS (22). IDR-1002 can also control immune-mediated inflammation in synovial fibroblasts, a key cell type in rheumatoid arthritis, by dampening the IL-1β response while promoting IL-1Ra and IL-10 production (19). The suppressive effect of IDR-1002 on IL-1β–induced inflammation is achieved by downregulating the activation of p50 NF-κB, JNK, and p38 MAPK (19). The dual effect of IDR-1002 has also been observed in LPS-stimulated macrophages, in which the peptide dampens the inflammatory response by inhibiting NF-κB nuclear translocation while activating p38/ERK1/2-MSK1–dependent CREB phosphorylation (20). Thus, IDR-1002 represents a potential anti-inflammatory and anti-infective therapeutic candidate because of its ability to dampen excessive inflammation without compromising the ability of the immune system to fight infections. Despite the promising anti-inflammatory activities of IDR-1002 observed during

Centre for Microbial Diseases and Immunity Research, Department of Microbiology and Immunology, University of British Columbia, Vancouver, British Columbia V6T 1Z4, Canada

ORCID: 0000-0002-4623-1934 (B.C.W.).

Received for publication July 10, 2017. Accepted for publication September 11, 2017.

This work was supported by Canadian Institutes of Health Research Grant MOP-74493.

B.C.W. and R.E.W.H. conceptualized the study; B.C.W. and A.H.-Y.L. performed the methods; B.C.W. performed most experiments; B.C.W. and A.H.-Y.L. performed formal analyses; B.C.W. wrote the original draft; all authors wrote, reviewed, and edited the manuscript; and R.E.W.H. acquired the funding.

The RNA transcriptomic data presented in this article have been submitted to the National Center for Biotechnology Information Gene Expression Omnibus (https://www.ncbi.nlm.nih.gov/geo/query/acc.cgi?acc=GSE100918) under accession number GSE100918.

Address correspondence and reprint requests to Dr. Robert E.W. Hancock, Centre for Microbial Diseases and Immunity Research, #232, 2259 Lower Mall Research Station, University of British Columbia, Vancouver, BC V6T 1Z4, Canada. E-mail address: bob@hancocklab.com

The online version of this article contains supplemental material.

Abbreviations used in this article: GPCR, G protein–coupled receptor; HDP, host defense peptide; IDR, innate defense regulator; Irf, IFN regulatory factor; LTA, lipoteichoic acid; RNA-Seq, sequencing of RNA after conversion to cDNA; RNS, reactive nitrogen species; ROS, reactive oxygen species.

bacterial infection, its role in controlling sterile inflammation has not been well characterized in vivo.

In this study, we showed that IDR-1002 suppressed the LPS-, lipoteichoic acid (LTA)-, and zymosan-induced inflammatory responses in vitro using RAW 264.7 cells. The effect of IDR-1002 peptide against sterile inflammation in vivo was investigated using the PMA-induced mouse ear inflammation model (23, 24). We demonstrated that IDR-1002 suppressed a variety of inflammatory responses, including PMA-induced ear edema, the production of proinflammatory cytokines, ROS, and reactive nitrogen species (RNS), and the recruitment of neutrophils into the inflamed tissue. We further explored the underlying mechanisms using systems biology approaches and showed that the in vivo suppressive effect of IDR-1002 on PMA-induced inflammation was contributed to by its ability to downregulate G-protein coupled receptors (GPCRs) in the class A/1 rhodopsin-like receptor family. These included receptors recognizing central proinflammatory mediators, such as chemokines, PGs, histamine, platelet-activating factor, and anaphylatoxin. We also found that IDR-1002 suppressed the IFN-γ pathway and an IFN regulatory factor (Irf)8-regulated network in PMA-induced inflammation.

Materials and Methods

Peptide and reagents

Peptide IDR-1002 (VQRWLIVWRIRK-NH_2) was synthesized by solid phase F-moc chemistry by Kinexus (Vancouver, BC). LTA (from *S. aureus*), zymosan (from *Saccharomyces cerevisiae*), PMA (≥99% TLC), indomethacin (≥99% TLC), protease inhibitor mixture, and phosphatase inhibitor mixture 2 were purchased from Sigma-Aldrich (St. Louis, MO). Penicillin-streptomycin (10,000 U/ml), L-glutamine (200 mM), DMEM, PBS and RNAlater RNA stabilization solution were obtained from Thermo Fisher Scientific (Waltham, MA). *Pseudomonas aeruginosa* PAO1 LPS was purified in-house, according to the protocol described in Darveau and Hancock (25).

RAW 264.7 cell culture and treatment

RAW 264.7 cells (passage numbers 3–15) were maintained in DMEM supplemented with 10% heat-killed FBS (Invitrogen), 2 mM L-glutamine, 100 U/ml penicillin, and 100 μg/ml streptomycin at 37°C and 5% CO_2. One milliliter containing 2×10^5 RAW 264.7 cells was seeded into each well of a 24-well plate (3524; Costar) and rested for 12 h before treatment. RAW 264.7 cells were treated with 5–100 ng/ml *P. aeruginosa* PAO1 LPS, 5–50 μg/ml *S. aureus* LTA, and 50–500 μg/ml *S. cerevisiae* zymosan, with or without 25 μg/ml IDR-1002, in fresh media. Culture supernatants were harvested 24 h posttreatment for the Griess assay and stored at −20°C for ELISA analysis.

Lactate dehydrogenase assay

The cytotoxicity of the LPS, LTA, and zymosan treatments, with or without 25 μg/ml IDR-1002, against RAW 264.7 cells was measured using a Cytotoxicity Detection Kit (Roche Diagnostics, Basel, Switzerland), according to the manufacturer's instructions. RAW 264.7 cell supernatants were collected and assessed 24 h posttreatment. Supernatants of untreated RAW 264.7 cells or RAW 264.7 cells lysed with 2% Triton X-100 were used as negative (0% toxicity) or positive (100% toxicity) control, respectively. The experiment was repeated five times.

Mice

All mouse experiments were performed according to the guidelines of the Canadian Council on Animal Care. The experimental protocol on animal studies was examined and approved by the University of British Columbia Animal Care Committee. CD-1 female mice (5 wk old) were purchased from Charles River Laboratories (Wilmington, MA). The mice were maintained at a controlled room temperature (22 ± 2°C) and humidity (40−60%) under a 14-h light and 10-h dark cycle for ≥1 wk before the experiments. Experimental and control mice were cohoused. Standard housing and animal care were provided by the Modified Barrier Facility at the University of British Columbia.

PMA-induced mouse ear inflammation model

To induce inflammation, 20 μl of 125 μg/ml PMA (i.e., 2.5 μg total) dissolved in acetone was applied topically onto both ears of CD-1 female mice (6–7 wk old). IDR-1002 (20 μl of 30 or 15 mg/ml in 50% ethanol) or indomethacin (20 μl of 30 or 15 mg/ml in acetone) was also administered topically within 3 min after PMA treatment onto one ear of each mouse. The contralateral ear was given the same volume of the vehicle/solvent (20 μl of 50% ethanol for mice given IDR-1002 and 20 μl of acetone for mice given indomethacin). Mice were euthanized 6 or 24 h post–PMA treatment for sample collection. The ear thickness was measured using a digital caliper. Blood samples were collected by cardiac puncture. Ear biopsies (5 mm in diameter) were cut out using disposable biopsy punches (VWR), weighed, and homogenized in 600 μl of extraction buffer (100 mM Tris [pH 7.4], 150 mM NaCl, 1 mM EGTA, 1 mM EDTA, 1% Triton X-100 and 0.5% sodium deoxycholate in autoclaved deionized water; protocol from Abcam, Toronto, Canada) supplemented with protease inhibitor mixture and phosphatase inhibitor mixture 2 (Sigma-Aldrich). Blood and homogenized tissue samples were centrifuged to collect serum and supernatants, respectively, for ELISA analysis. For sequencing of RNA after conversion to cDNA (RNA-Seq), ear biopsies (5 mm in diameter) were harvested, immediately submerged in RNAlater RNA stabilization solution (Thermo Fisher), and stored at −80°C until RNA isolation.

In vivo imaging

In vivo imaging was performed 6 h posttreatment. To visualize ROS/RNS production, we adapted and modified the protocol from van der Plas et al. (26). In brief, mice were injected s.c. with the luminescence probe L-012 (25 mg/kg; Wako Chemicals) dissolved in 50% PBS and imaged using an IVIS Spectrum (Caliper Life Sciences) 20–30 min postinjection under 2% isoflurane anesthesia. Images were acquired using Living Image version 3.1 (Caliper Life Sciences) with 45-s exposure time. To detect neutrophil recruitment, mice were injected i.v. with the Neutrophil Specific, NIR Fluorescent Imaging Agent (0.1 μmol/kg; Kerafast) and imaged using an IVIS Spectrum (Caliper Life Sciences) 3 h postinjection under 2% isoflurane anesthesia. Images were acquired using Living Image version 3.1 (Caliper Life Sciences) under autoexposure, with the fluorescent filter setting at 745 nm for excitation and 800 nm for emission.

Histology

For histological assessment, ear biopsies (5 mm in diameter) were collected 6 h posttreatment and fixed in 10% neutral-buffered formalin solution. H&E staining was conducted by Wax-it Histology Services (Vancouver, BC, Canada). The numbers of immune cells per high-power field (400× magnification) in the stained specimens were quantified by an independent pathologist.

ELISA

Mouse TNF-α, IL-6, and MCP1 ELISA kits were purchased from eBioscience (San Diego, CA). A Mouse CXCL1 (KC) ELISA Kit was obtained from R&D Systems (Minneapolis, MN). A Histamine ELISA Kit was from Enzo Life Sciences (Brockville, ON, Canada). The concentrations of TNF-α and IL-6 in RAW 264.7 cells were measured from five independent experiments. IL-6, MCP1, and CXCL1 levels in mice ear tissue and serum were quantified from 14–23 mice per peptide concentration. Histamine concentrations in mouse ear tissue and serum were determined from three to five mice per peptide concentration, according to the manufacturer's instructions.

Griess assay

Griess reagent (modified) was purchased from Sigma-Aldrich. Equal volumes of 1× Griess reagent were mixed with Griess standards or RAW 264.7 cell supernatant harvested 24 h posttreatment. The absorbance at 540 nm was determined using a microplate reader (PowerWave 340) after a 15-min incubation at room temperature. The experiment was repeated five times.

RNA-Seq analysis

Tissue biopsies were taken from 15 mice 6 h posttreatment: 5 vehicle control mice (20 μl acetone and 20 μl 50% ethanol), 4 PMA-treated mice (20 μl of 125 μg/ml PMA and 20 μl of 50% ethanol), and 6 mice treated with PMA and IDR-1002 (20 μl of 125 μg/ml PMA and 20 μl of 30 mg/ml IDR-1002). Total RNA from each sample was extracted using an RNeasy Mini Kit (QIAGEN), following the manufacturer's protocol. For quality control, 1 μl of each sample was run on the Agilent 2100 Bioanalyzer using a Eukaryotic Total RNA Nano Chip (Agilent Technologies).

To construct libraries, 2 μg of each RNA sample was used. Poly-A tailed RNA enrichment was done using a Magnetic mRNA Isolation Kit (New England Biolabs). cDNA library preparation was done using a KAPA

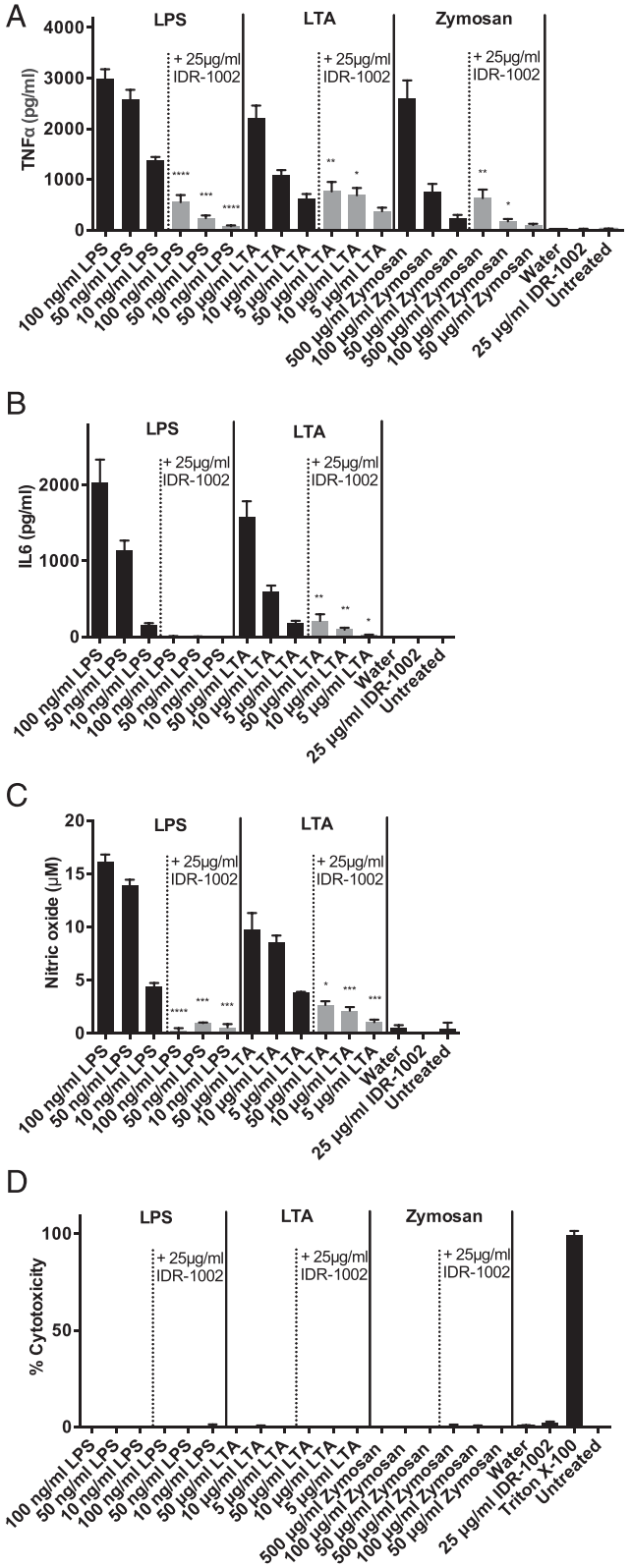

FIGURE 1. IDR-1002 dampened LPS-, LTA-, and zymosan-induced inflammatory responses in RAW 264.7 cells. RAW 264.7 cells were treated with different concentrations of LPS, LTA, and zymosan in the absence or presence of 25 μg/ml IDR-1002. Culture supernatants were harvested 24 h posttreatment. The concentrations of TNF-α (**A**) and IL-6 (**B**) were determined by ELISA, and the concentration of NO (**C**) was quantified by the Griess assay. (**D**) Cytotoxicity was determined using the lactate dehydrogenase assay. Supernatants from untreated RAW 264.7 cells or RAW 264.7 cells lysed with 2% Triton X-100 were used as negative (0% toxicity) or positive (100% toxicity) control, respectively. Data shown were an average of five independent replicates, and error bars were calculated as the SEM. Statistical analysis comparing peptide-treated or untreated RAW 264.7 cells challenged with the same concentration of each stimulus was performed using a Student unpaired *t* test with the Welch correction. $*p \leq 0.05$, $**p \leq 0.01$, $***p \leq 0.001$, $****p \leq 0.0001$.

Stranded Total RNA Kit (Kapa Biosystems). In brief, mRNAs were enzymatically fragmented, followed by first- and second-strand cDNA synthesis. Overhangs were repaired and adenylated to produce blunt ends, and unique indices were ligated. DNA libraries were amplified by PCR, followed by cleaning and size selection using an AMPure XP Kit (Agencourt). DNA samples were quantified using a Quant-iT dsDNA Assay Kit (Invitrogen) and normalized to 4 nM. Samples were then pooled and sequenced on a HiSEquation 2500 sequencer (Illumina), using the high-output mode, at the University of British Columbia Sequencing Centre.

Sequenced data quality control was performed using FastQC v0.11.5 and MultiQC v0.8.dev0 (27). Sample libraries were then aligned to mouse genome Ensembl GRCm38 (28) using STAR v2.5 (29). The median of uniquely mapped reads was ~6 million per sample. A read count table was generated using HTSeq-count v0.6.1p1 (30), and genes that had <10 counts were removed. Differential expression analysis was performed using DESeq2 v1.14.0 (31). Pathway enrichment was carried out using Sigora v2.0.1 (32), and network analysis was done by NetworkAnalyst (33). The genes in various inflammatory pathways were downloaded from InnateDB (34). For RNA-Seq analysis, the cutoff used for differentially expressed genes was ≥2-fold, with a *p* value adjusted for multiple testing ≤ 0.05. Statistical analysis for pathway enrichment was performed using a hypergeometric test and corrected for multiple comparisons by the Bonferroni method, with a cutoff of $p \leq 0.001$.

Statistical analyses

Statistical significance for in vitro and in vivo protein experiments was determined using GraphPad Prism. Comparison between two groups was performed using the Student unpaired *t* test with the Welch correction.

Results

IDR-1002 peptide dampened LPS-, LTA-, and zymosan-induced inflammatory responses in RAW 264.7 cells

Initial studies on the anti-inflammatory effect of IDR-1002 were carried out in vitro using RAW 264.7 murine monocyte/macrophage cells challenged with the TLR4 agonist LPS and the TLR2 agonists LTA and zymosan. These stimuli had defined compositions, acted through known pathways, and had been used to trigger inflammation in published mouse acute ear inflammation models (23). LPS and LTA triggered TNF-α, IL-6, and NO production in a dose-dependent manner, whereas zymosan only induced a TNF-α response at 24 h poststimulation (Fig. 1A–C). The addition of 25 μg/ml IDR-1002 led to significant suppression of LPS-induced, LTA-induced (at 50 and 10 μg/ml), and zymosan-induced (at 500 and 100 μg/ml) TNF-α production. IDR-1002 also significantly dampened IL-6 and NO production triggered by LPS and LTA. In particular, 25 μg/ml IDR-1002 completely abolished the LPS-induced IL-6 response. The stimuli and peptide treatments were not cytotoxic toward RAW 264.7 cells, as determined using a lactate dehydrogenase assay (Fig. 1D). The anti-inflammatory activity of IDR-1002 occurred at even lower concentrations, and 5 μg/ml caused a 77% decrease in LPS-stimulated TNF-α production by RAW264.7 cells, consistent with previous data on human cells (21). These results confirmed and extended previous data (19–21) indicating that IDR-1002 peptide effectively suppressed sterile inflammatory responses in vitro. We also tested PMA; however, this agent was quite toxic in vitro and did not trigger TNF-α, IL-6, or NO production within the concentration range (≤1 μg/ml) that was nontoxic to RAW 264.7 cells.

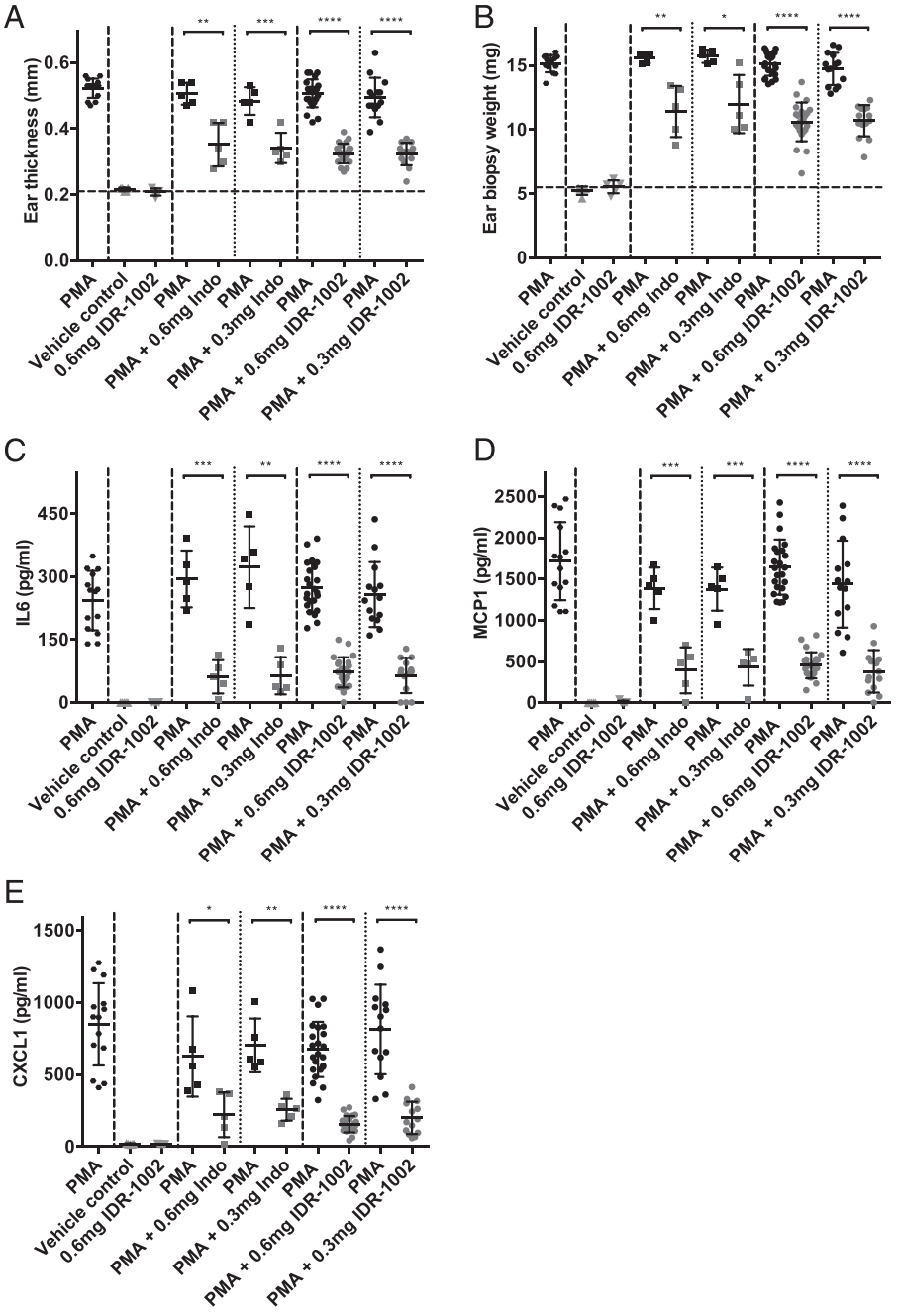

FIGURE 2. IDR-1002 suppressed PMA-induced ear edema and the production of proinflammatory cytokine IL-6 and chemokines MCP1 and CXCL1 in PMA-inflamed ear tissue. Ears of CD-1 mice were treated topically with 20 μl of 125 μg/ml PMA. Either 0.6 or 0.3 mg of IDR-1002 was administered onto one ear of each mouse immediately after PMA treatment. Indomethacin (Indo), at a dose of 0.6 or 0.3 mg per ear, was used as positive anti-inflammatory control and was also applied topically onto one ear of each mouse post–PMA treatment. The contralateral ears were given the same volume of the vehicle/solvent (20 μl of 50% ethanol for mice given IDR-1002 and 20 μl of acetone for mice given indomethacin). Mice were euthanized 6 h post–PMA treatment, and increases in ear thickness (**A**) and ear weight (**B**) were quantified. Ear biopsy was collected and homogenized for IL-6 (**C**), MCP1 (**D**), and CXCL1 (**E**) measurement using ELISA. *$p \leq 0.05$, **$p \leq 0.01$, ***$p \leq 0.001$, ****$p \leq 0.0001$, Student unpaired *t* test with the Welch correction.

IDR-1002 suppressed the production of proinflammatory cytokines and chemokines in vivo

To investigate the anti-inflammatory activity of IDR-1002 on sterile inflammation in vivo, we used the well-established PMA-induced mouse ear inflammation model. The topical administration of 20 μl of 125 μg/ml PMA onto the ears of female CD-1 mice caused a strong inflammatory reaction, as revealed by a nearly 3-fold increase in ear thickness and biopsy weight compared with ears treated with vehicle control or peptide control. PMA also triggered strong production of the proinflammatory cytokine IL-6 (243 ± 71 pg/ml [mean ± SD]) and the chemokines MCP1 (1718 ± 474 pg/ml) and CXCL1 (849 ± 286 pg/ml) in the ear tissue. The effect of IDR-1002 treatment was evaluated by applying 0.6 or 0.3 mg of peptide topically onto one ear of each mouse immediately after PMA challenge. Matching doses of the nonsteroidal anti-inflammatory drug indomethacin were used as positive controls, whereas the addition of vehicles (solvents) served as negative controls and were also applied topically after PMA treatment. At 6 h posttreatment, IDR-1002 significantly ($p < 0.0001$) suppressed the increase in ear thickness and ear weight induced by PMA to an equivalent extent as the positive control indomethacin (Fig. 2A, 2B). Peptide treatment also consistently and significantly ($p < 0.0001$) dampened the production of IL-6, MCP1, and CXCL1 in the ear tissue (Fig. 2C–E). PMA caused only modest changes in serum cytokine levels, and neither indomethacin nor peptide IDR-1002 significantly altered the cytokine levels in mouse serum at 6 h (Supplemental Fig. 1A, 1C, 1E).

The anti-inflammatory effect of IDR-1002 on ear inflammation was also measured at 24 h post–PMA treatment (Fig. 3). IDR-1002 treatment led to suppression of ear tissue edema almost to the level of the vehicle-treated control, suggesting resolution of inflammation within 24 h (Fig. 3A, 3B). In addition, peptide treatment completely inhibited the production of IL-6, MCP1, and

CXCL1 in the ear tissue (15 mice per peptide concentration, Fig. 3C–E). Similar to the 6-h treatment, IDR-1002 by itself did not significantly alter cytokine and chemokine levels in the mouse serum 24 h post–PMA treatment (Supplemental Fig. 1B, 1D, 1F). These results indicated that a single topical treatment of IDR-1002 suppressed PMA-induced acute inflammation by downregulating proinflammatory cytokine production at early stages of inflammation and resolving local inflammation within 24 h.

IDR-1002 dampened the production of ROS/RNS and attenuated neutrophil infiltration in vivo

The overproduction of ROS and RNS can induce oxidative and nitrosative stress responses, which contribute to a variety of pathological processes, including inflammatory diseases (35). We investigated whether PMA triggered these responses and whether IDR-1002 could dampen ROS/RNS production by s.c. injection of a luminescent probe L-012, which allows visualization of ROS/RNS (26, 36). PMA led to potent induction of local ROS/RNS production (Fig. 4A), whereas administration of vehicle or IDR-1002 on the contralateral ear led to no induction of these species. IDR-1002 treatment at both doses (0.6 and 0.3 mg per ear) dampened the production of ROS/RNS in the PMA-inflamed ear tissue, as shown by substantially diminished luminescence signals after in vivo imaging (Fig. 4A). Because neutrophils are one of the dominant cell types mediating acute PMA-induced inflammation and a major source of ROS (37, 38), we also monitored neutrophil levels by in vivo imaging using the Neutrophil Specific, NIR Fluorescent Imaging Agent, a cyanine7-conjugated polyethylene glycol–modified hexapeptide that binds specifically to the formylpeptide receptor of neutrophils (39). PMA caused a strong local (ear tissue) neutrophil influx after 6 h, which was almost completely attenuated by peptide treatment (Fig. 4B).

IDR-1002 reduced PMA-induced ear edema and modulated immune cell composition in vivo

Because increases in ear thickness, weight, and redness were triggered by topical PMA treatment, H&E staining was used to further study ear edema and the effect of IDR-1002 on tissue

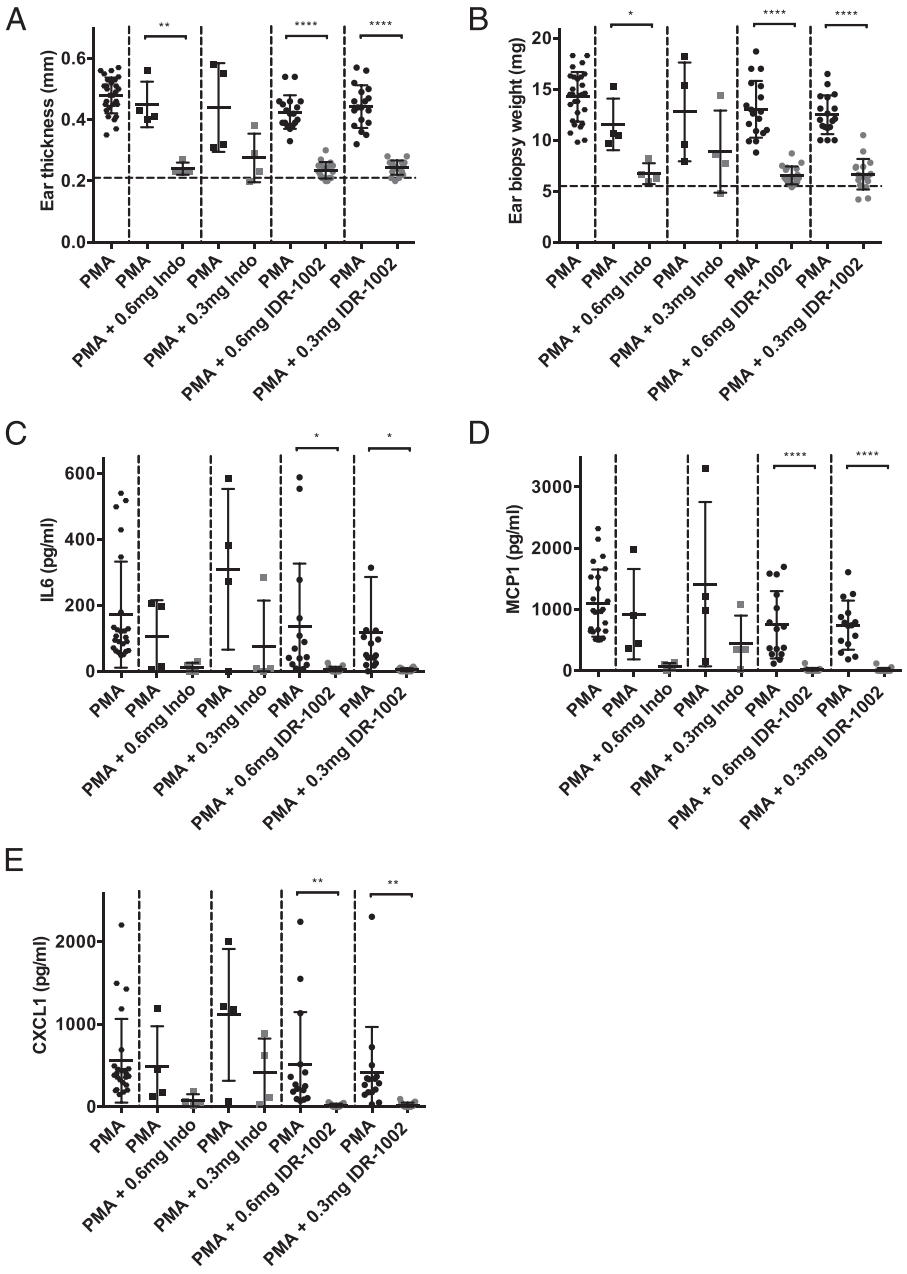

FIGURE 3. By 24 h, IDR-1002 almost completely suppressed PMA-induced ear edema and the production of proinflammatory cytokine and chemokines in PMA-inflamed ear tissue. Ears of CD-1 mice were treated as mentioned in Fig. 2. Mice were euthanized 24 h post–PMA treatment, and increases in ear thickness (**A**) and ear weight (**B**) were quantified. Ear biopsy was collected and homogenized for IL-6 (**C**), MCP1 (**D**), and CXCL1 (**E**) measurement using ELISA. *$p \leq 0.05$, **$p \leq 0.01$, **** $p \leq 0.0001$, unpaired Student t test with the Welch correction.

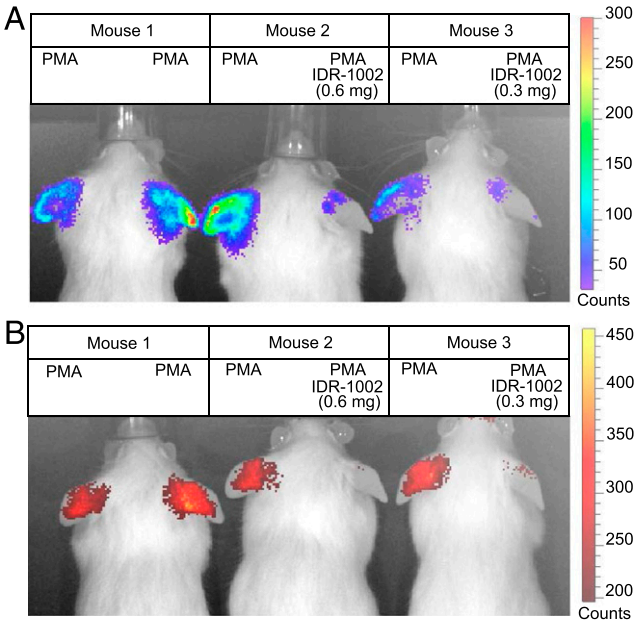

FIGURE 4. IDR-1002 dampened the production of ROS/RNS and attenuated neutrophil infiltration in the PMA-inflamed ear tissue. Ears of CD-1 mice were treated topically with IDR-1002 and/or 20 μl of 125 μg/ml PMA. (**A**) In vivo imaging was performed 6 h posttreatment. To visualize ROS/RNS production, mice were injected s.c with the luminescent probe L-012 (25 mg/kg; Wako Chemical) and imaged using an IVIS Spectrum 20–30 min postinjection. (**B**) To detect neutrophil recruitment, mice were injected i.v. with the Neutrophil-Specific, NIR Fluorescent Imaging Agent (0.4 mg/kg; Kerafast) and imaged using an IVIS Spectrum 3 h postinjection.

structure and immune cell composition (Fig. 5). Compared with administration of vehicle control or IDR-1002 alone, PMA treatment resulted in substantial thickening of the ear as the result of a massive recruitment of immune cells and accumulation of interstitial fluid in the dermal layer of the ear tissue. The suppressive effects of IDR-1002 on inflammation were seen by decreases in immune cell density and relative ear thickness (Fig. 5A). The stained sections were scored by an independent pathologist. Consistent with the in vivo imaging results (Fig. 4B), peptide treatment significantly decreased the number of neutrophils present in the PMA-treated ear tissue by up to 10-fold (Fig. 5B). Interestingly, under inflammatory conditions, IDR-1002 treatment resulted in a nearly 2-fold increase in eosinophils (Fig. 5C) and a 2.5-fold increase in mast cells (Fig. 5D). Although these increases were modest [cf. eosinophilic esophagitis in which the eosinophil counts can range from 1 to >400 per high-power field (40)], we were concerned that the appearance of these cells was associated with an allergic reaction. Therefore, we examined the levels of histamine in mouse ear tissue and serum. No significant changes in histamine levels were observed 15 min or 1 and 6 h after peptide treatment (Supplemental Fig. 2).

RNA-Seq analysis of IDR-1002 suppression of PMA-induced inflammation

To gain a more comprehensive understanding of the anti-inflammatory mechanism of IDR-1002, RNA-Seq analysis was performed on RNA samples extracted from mouse ear tissue at 6 h posttreatment with vehicle, PMA alone, or PMA followed immediately by IDR-1002. Genes were considered differentially expressed if they had an expression change ≥ 2-fold or ≤ 0.5-fold, with an adjusted p value ≤ 0.05. Pathway enrichment analysis using Sigora v2.0.1 (32) considered only those overrepresented pathways with an adjusted p value ≤ 0.001. PMA treatment induced tremendous transcriptomic changes, with 2270 upregulated genes representing 36 pathways and 2048 downregulated genes representing 14 pathways (Table I). The top upregulated pathways compared with vehicle control were known inflammatory pathways involved in cytokine signaling (adjusted p value 1.63×10^{-195}), especially IFN-γ (1.47×10^{-153}), TNF-α (4.28×10^{-21}), and IL-1 (6.62×10^{-17}) signaling; chemokine receptor activation (3.50×10^{-150}); class A/1 rhodopsin-like receptor cascade (1.88×10^{-63}); cell surface interactions at the vascular wall (3.23×10^{-81}); hemostasis (1.66×10^{-65}); and various TLR signaling pathways. Among these pathways, TNF-α and IL-1 responses have well-established roles in mediating sterile inflammation (2, 3, 5). In addition, the IFN-γ pathway and the integrin-mediated cell adhesion process were previously found to be essential for PMA-induced inflammation (41–44). Pathways downregulated by PMA included those involved in WNT ligand biogenesis, trafficking (1.89×10^{-06}), and signaling (2.92×10^{-06}), which are known to orchestrate cell proliferation, differentiation, and migration during skin organogenesis (45, 46).

To characterize the mechanism of action of IDR-1002 on PMA-induced inflammation, we compared PMA challenge and IDR-1002 treatment with PMA challenge alone and observed significant downregulation of chemokine receptors (4.95×10^{-99}) in the class A/1 rhodopsin-like GPCR family (9.12×10^{-45}), cytokine signaling (7.58×10^{-21}), especially IFN-γ (3.15×10^{-38}), and pattern recognition receptor cascades, such as C-type lectin receptors (2.60×10^{-13}), TLR1-2 heterodimer (4.21×10^{-05}), and TLR10 (3.30×10^{-05}) (Table II). Consistent with the in vivo imaging and histology results indicating that IDR-1002 attenuated PMA-induced immune cell infiltration, the signaling pathway involved in leukocyte extravasation (cell surface interactions at the vascular wall 4.57×10^{-71}) was also substantially downregulated by IDR-1002. In contrast, a subset of class A/1 rhodopsin-like receptors (4.10×10^{-06}) involved in neurotransmission, ion and nutrient transportation, and gene function in WNT signaling (4.32×10^{-04}) were upregulated in the PMA-inflamed ear treated with IDR-1002 compared with PMA alone.

IDR-1002 downregulated a variety of class A/1 rhodopsin-like receptors functioning in inflammation

Class A/1 rhodopsin-like receptors are the major family of GPCRs and play important roles in the sensing and cellular communication processes of inflammation (47). Therefore, we further probed the effect of IDR-1002 on the expression of chemokines and their receptors during sterile inflammation. Combined PMA and IDR-1002 treatment compared with PMA challenge downregulated chemokine receptors and their ligands for neutrophils (e.g., Cxcr1, Cxcr2, Cxcl1, Cxcl2, Cxcl3 and Cxcl5), eosinophils (e.g., Ccl11), monocytes (e.g., Ccl7), and other chemokines attracting multiple cell types (e.g., Ccl3 and Ccl5) (Fig. 6). In addition, class A/1 rhodopsin-like receptors recognizing other proinflammatory mediators, such as PGs (e.g., Ptger2 and Ptgir), histamine (e.g., Hrh2), platelet-activating factor (e.g., Ptafr), and anaphylatoxin C3a (e.g., C3ar1), were also downregulated by IDR-1002. These results were consistent with the hypothesis that IDR-1002 acted by attenuating the migration and accumulation of inflammatory cells and controlled vascular endothelial permeability by modulating the expression of class A/1 rhodopsin-like receptors.

IDR-1002 dampened inflammation by suppressing an Irf8-regulated network

Irf8 is a transcription factor that is restricted primarily to hematopoietic cells and often acts by associating with other transcription factors to modulate key inflammatory responses, including the

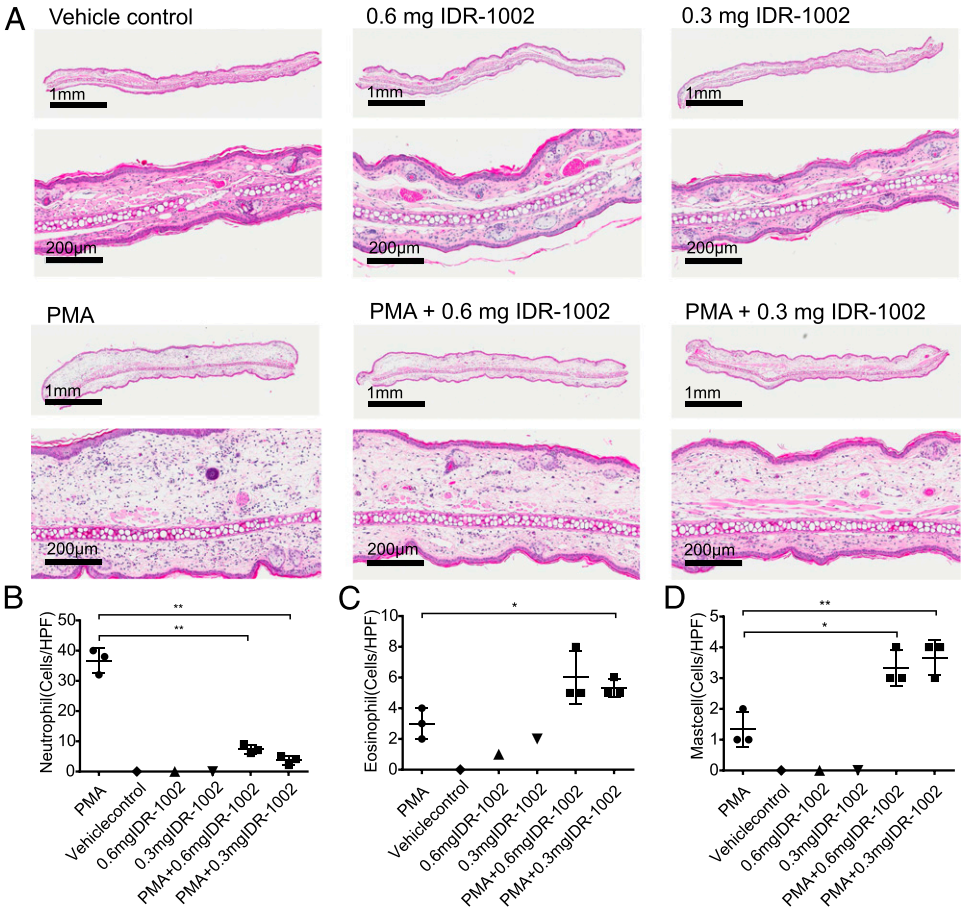

FIGURE 5. IDR-1002 reduced PMA-induced ear edema and attenuated neutrophil recruitment in the PMA-inflamed ear tissue. Ears of CD-1 mice were treated topically with IDR-1002 and/or 20 μl of 125 μg/ml PMA. Mice were euthanized 6 h post–PMA treatment, and ear biopsies were collected and fixed in 10% buffered formalin. (**A**) H&E staining was performed by Wax-it Histology Services. (**B–D**) The numbers of immune cells per high-power field (HPF) in the stained specimens were quantified by a pathologist. $*p \leq 0.05$, $**p \leq 0.01$, by unpaired Student *t* test with the Welch correction.

IFN-γ response, TLR signaling, and the expression of inducible NO synthase (48, 49). When comparing PMA and IDR-1002 combined treatment with PMA challenge, Irf8 was identified to be one of the central hubs in the zero-order protein–protein interaction network, interacting with 28 other transcriptionally dysregulated proteins (27 of which were upregulated by PMA and suppressed in the presence of IDR-1002 treatment) (Fig. 7). These interactors included Tlr4, Tnf and Nlrp3, each of which play central roles in inflammatory signaling and cytokine production, as well as proteins involved in the recruitment (e.g., Ccl5, Ccl6 and Itga5) and function (e.g., Slc11a1/Nramp, Csf3r, and Ncf1) of inflammatory cells, including macrophages and neutrophils (50–53). Each of these 28 protein interactors has been previously shown to have Irf8 binding sites and are regulated by Irf8 and its transcription factor partners (54–57). For example, Irf8 works in cooperation with transcription factors Irf1, NF-κB, and PU.1 to promote chemokine Ccl5 expression in response to IFN-γ and LPS (55). Irf8 and Irf1 are also involved in IFN-γ–induced TNF-α expression (57). Furthermore, Irf8 participates in the transcriptional regulation of the LPS-induced TLR4 cascade and the crosstalk between TLR4 signaling and the IFN-γ response (48, 56). Because Irf8 plays a critical role in upregulating inflammation in cooperation with various transcription factors, we propose that IDR-1002 acts to control a variety of inflammatory responses by suppressing the induction of Irf8 and its target genes, such as Ccl5, TNF, and TLR4. Thus, these results provided key insights into the anti-inflammatory mechanism of IDR-1002.

Discussion

Dysregulated inflammation is a well-known pathological factor at the root of many human disorders and represents a major threat to human health and welfare (58). HDPs and IDRs possess encouraging therapeutic potential as a result of their ability to modulate the immune response to increase protective immunity while dampening inflammation (16, 59). In this study, we focused on peptide IDR-1002, which has been demonstrated to promote in vivo protective innate immunity to infections, dampen proinflammatory cytokine responses to inflammatory agonists, and promote protective adaptive immunity as a component of adjuvant formulations (18–22, 60). Our data indicate its potent ability to antagonize sterile inflammation.

The in vitro studies were carried out using RAW 264.7 cells, and we showed that IDR-1002 significantly suppressed LPS- and LTA-induced TNF-α, IL-6, and NO production, as well as the zymosan-induced TNF-α response (Fig. 1A–C), without harming RAW 264.7 cell membrane integrity (Fig. 1D). Previous studies showed that IDR-1002 reduced the LPS-induced inflammation in human PBMCs (21). Our observation that IDR-1002 reduced TLR4 and TLR2 agonist-induced inflammation was consistent with this finding and extended the scope of inflammatory agonists that IDR-1002 could antagonize.

To further investigate the anti-inflammatory activities of IDR-1002 in vivo, we used the PMA-induced mouse ear inflammation model, a well-established model for screening the activities of many anti-inflammatory drugs (23). PMA treatment induced strong inflammatory responses, as observed by increases in ear thickness, ear weight, and proinflammatory cytokine production locally (in ear tissue) and, to a limited extent, systemically (in serum). Topical IDR-1002 treatment suppressed proinflammatory cytokine production in the PMA-inflamed ear tissue comparably to the nonsteroidal anti-inflammatory drug indomethacin at 6 h posttreatment (Fig. 2). In addition, IDR-1002 completely inhibited

Table I. Pathways dysregulated by PMA challenge compared with vehicle control

Pathway Description	Corrected p Values
Upregulated pathways	
Cytokine signaling in immune system	1.63×10^{-195}
IFN-γ signaling	1.47×10^{-153}
Chemokine receptors bind chemokines	3.50×10^{-150}
Cell surface interactions at the vascular wall	3.23×10^{-81}
Hemostasis	1.66×10^{-65}
Class A/1 (rhodopsin-like receptors)	1.88×10^{-63}
MyD88-independent TLR3/TLR4 cascade	1.37×10^{-36}
C-type lectin receptors	3.34×10^{-25}
TLR5 cascade	9.24×10^{-25}
Immunoregulatory interactions between a lymphoid and a nonlymphoid cell	1.98×10^{-22}
TNFs bind their physiological receptors	4.28×10^{-21}
DAP12 interactions	$8.00 \times 10_{-19}$
IL-1 signaling	6.62×10^{-17}
IFN signaling	9.94×10^{-16}
Signaling by ILs	6.52×10^{-15}
TLR10 cascade	2.83×10^{-14}
Activated TLR4 signaling	1.72×10^{-13}
Ag activates BCR leading to generation of second messengers	1.27×10^{-12}
TNFR superfamily members mediating noncanonical NF-κB pathway	3.82×10^{-10}
PI3K cascade	5.03×10^{-10}
VEGFA-VEGFR2 pathway	2.98×10^{-09}
Sema4D-induced cell migration and growth-cone collapse	3.30×10^{-09}
Activation of NF-κB in B cells	3.00×10^{-8}
Amino acid transport across the plasma membrane	6.30×10^{-8}
MyD88 cascade initiated on plasma membrane	1.03×10^{-7}
TLR1:TLR2 cascade	7.11×10^{-7}
IRS-related events triggered by IGF1R	3.11×10^{-6}
ARMS-mediated activation	6.10×10^{-6}
Formyl peptide receptors bind formyl peptides and many other ligands	1.03×10^{-5}
Sema4D in semaphorin signaling	2.47×10^{-5}
Gap junction trafficking	2.53×10^{-5}
RHO GTPases activate NADPH oxidases	2.53×10^{-5}
EPHB-mediated forward signaling	4.21×10^{-5}
Hyaluronan uptake and degradation	1.39×10^{-4}
Semaphorin interactions	2.25×10^{-4}
Signaling by VEGF	8.47×10^{-4}
Downregulated pathways	
Phase 1: functionalization of compounds	1.12×10^{-17}
Negative regulation of TCF-dependent signaling by WNT ligand antagonists	1.52×10^{-15}
Cell cycle, mitotic	1.02×10^{-14}
Anchoring of the basal body to the plasma membrane	2.07×10^{-12}
Rho GTPase cycle	2.26×10^{-11}
G α (s) signaling events	9.12×10^{-8}
Assembly of the primary cilium	1.33×10^{-7}
Signaling by Rho GTPases	3.87×10^{-7}
Regulation of FZD by ubiquitination	5.05×10^{-7}
WNT ligand biogenesis and trafficking	1.89×10^{-6}
Signaling by WNT	2.92×10^{-6}
Intraflagellar transport	2.79×10^{-4}
ABC family proteins mediated transport	7.30×10^{-4}
Axon guidance	7.87×10^{-4}

RNA-Seq analysis was performed on the ear tissue from 15 mice 6 h posttreatment. Differential expression analysis was performed using DESeq2 v1.14.0 with a threshold of 2-fold changes. Pathway enrichment was carried out using Sigora v2.0.1. Statistical analysis was performed using a hypergeometric test, and multiple comparisons were corrected by the Bonferroni method, with a cutoff of $p \leq 0.001$.

Table II. Dysregulated pathways comparing IDR-1002 treatment of PMA-induced inflammation to PMA challenge alone

Pathway Description	Corrected p Values
Upregulated pathways	
Chemokine receptors bind chemokines	4.95×10^{-99}
Cell surface interactions at the vascular wall	4.57×10^{-71}
Class A/1 (rhodopsin-like receptors)	9.12×10^{-45}
IFN-γ signaling	3.15×10^{-38}
Peptide ligand–binding receptors	1.91×10^{-37}
DAP12 interactions	8.99×10^{-22}
Cytokine signaling in immune system	7.58×10^{-21}
Hemostasis	2.26×10^{-20}
C-type lectin receptors	2.60×10^{-13}
Hyaluronan uptake and degradation	9.10×10^{-6}
TLR10 cascade	3.30×10^{-5}
TLR1:TLR2 cascade	4.21×10^{-5}
IRS-related events triggered by IGF1R	6.98×10^{-4}
Downregulated pathways	
Class A/1 (rhodopsin-like receptors)	4.10×10^{-6}
WNT ligand biogenesis and trafficking	4.32×10^{-4}

RNA-Seq analysis was performed on the ear tissue of 15 mice at 6 h posttreatment. Differential expression analysis was performed using DESeq2 v1.14.0 with a threshold of 2-fold changes. Pathway enrichment was carried out using Sigora v2.0.1. Statistical analysis was performed using a hypergeometric test, and multiple comparisons were corrected by the Bonferroni method with a cutoff of $p \leq 0.001$.

PMA-induced IL-6, MCP1, and CXCL1 production locally within 24 h (Fig. 3). Indomethacin is a potent anti-inflammatory agent with many serious side effects. For example, indomethacin increases the risk for cardiovascular thrombotic events, gastrointestinal ulceration, and skin rashes (61, 62). In particular, neutrophils and ROS have been reported to play crucial roles in the development of indomethacin-induced gastric mucosal injury (63). IDR-1002 peptide was previously shown to modulate neutrophil degranulation, adhesion, and ROS production in vitro (22). Using in vivo imaging techniques, we were able to monitor real-time ROS/RNS levels. The imaging results showed that IDR-1002 could effectively dampen the production of ROS/RNS, likely by attenuating neutrophil infiltration (Fig. 4). The reduction in the neutrophil population in the PMA-inflamed ear tissue was confirmed by a histology study in which peptide treatment significantly decreased the number of neutrophils per high-power field (Fig. 5). Interestingly, although H&E staining indicated an increase in the eosinophil and mast cell density, this was not accompanied by increases in histamine release (Supplemental Fig. 2), a deleterious effect observed for several other HDPs, including hBD-2 and LL-37 (64). Together, these results demonstrate a potential advantage of IDR-1002 as an anti-inflammatory drug candidate. Future experiments will focus on confirming the safety and efficiency of IDR-1002 under more human-mimicking conditions. For example, the activities of IDR-1002 will be tested using an ex vivo human skin model or in the presence of human blood plasma.

Using RNA-Seq analysis, we were able to study the global transcriptomic changes, avoiding bias toward specific pathways and oversimplifying the biological outputs. Pathway analysis revealed that 36 pathways were significantly upregulated in the PMA-treated ear tissue (Table I). These include IFN-γ, TNF, and IL-1 cascades, which are at the core of many autoinflammatory and autoimmune disorders, such as systemic lupus erythematosus, rheumatoid arthritis, and atherosclerosis (65–68). TLR signaling, which is known to initiate and perpetuate nonmicrobial inflammatory responses triggered by damage-associated molecular patterns, was also upregulated by PMA treatment (2, 69). Differential gene expression analysis revealed that most of the genes were downregulated by IDR-1002 under PMA-induced inflammatory conditions. These genes belonged to many of the inflammatory pathways upregulated in response to PMA, such as the chemokine

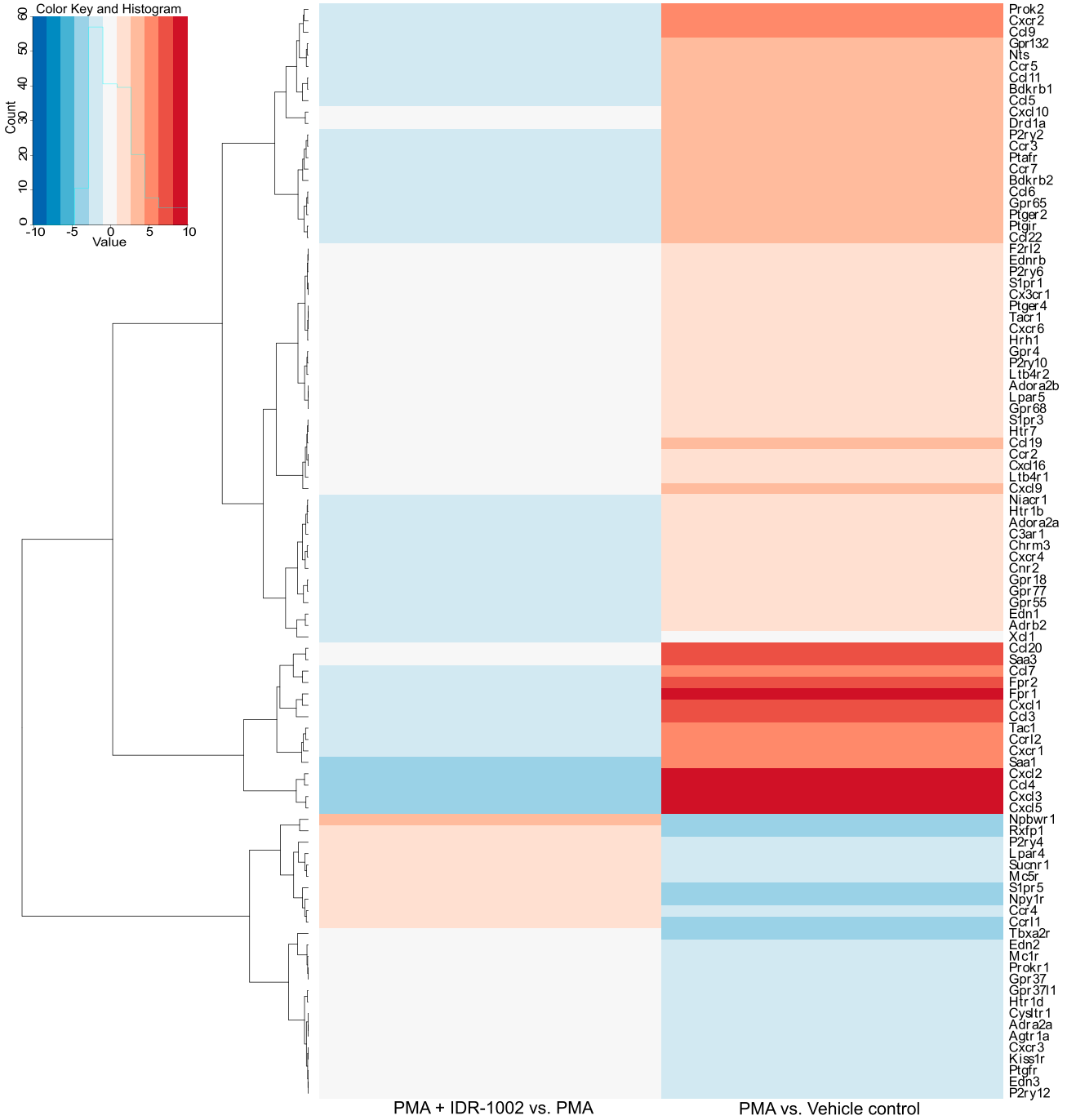

FIGURE 6. Heat map of differentially expressed genes from the GPCR receptor (class A/1 rhodopsin-like) pathway in response to PMA-induced inflammation, with or without IDR-1002 treatment. Genes were downloaded from InnateDB. The heat map of differentially expressed genes (≥2-fold change, adjusted p value ≤ 0.05) was generated using R v.3.3.3, qplot package. Red indicates upregulation, and blue indicates downregulation.

receptors–binding chemokine pathway, cell surface interactions at the vascular wall, class A/1 rhodopsin-like receptors, and IFN-γ signaling (Table II). A key limitation of this approach is that the gene expression occurred in the diverse population of cells in the ear and could not be accurately associated with any particular cell type. An estimate of the changes in ear tissue cell populations was obtained by the frequency of appearance of cell markers in the RNA-Seq dataset (Supplemental Table I). When comparing PMA and IDR-1002 combined treatment with PMA challenge alone, we observed a significant decrease in macrophage or monocyte, dendritic cell, neutrophil, and NK cell markers and an increase in mast cell markers. However, these apparent changes in cell number were insufficient to fully explain the large number and, in some instances, high fold changes of genes differentially regulated by IDR-1002 treatment. Therefore, the anti-inflammatory effect of IDR-1002 was likely achieved by modulating both the functions and numbers of the ear tissue cell populations.

Topical application of PMA onto mouse ears is known to provoke PG and leukotriene biosynthesis, which leads to increased vascular permeability and evokes infiltration of inflammatory cells, including neutrophils (37, 70, 71). Comparing IDR-1002–treated with untreated PMA-inflamed ear tissue, we observed substantial suppression of a variety of class A/1 rhodopsin-like receptors, the largest group of GPCRs, including, but not limited to, receptors

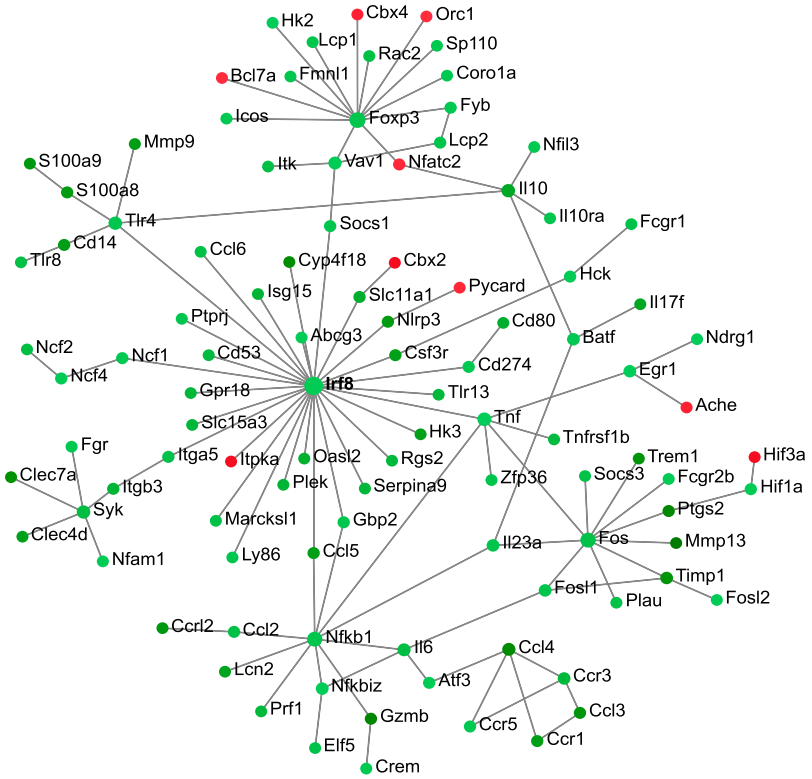

FIGURE 7. Network analysis of IDR-1002 suppression of PMA-induced ear inflammation. Zero order protein–protein interaction network comparing combined PMA and IDR-1002 treatment with PMA challenge alone using NetworkAnalyst. Red nodes denote upregulation, and green nodes denote downregulation.

for neutrophils, PGs, histamine, platelet-activating factor, and anaphylatoxin (Fig. 6). Previous studies have shown that IDR peptides can interact with GPCRs on the cell surface and thereafter modulate immune cell functions (16). In particular, IDR-1002 can enhance chemokine production and promote neutrophil infiltration in response to bacterial infections (18). Our results suggest that, during sterile inflammation, controlling GPCR expression, especially suppressing the expression of chemokine and chemokine receptors, might be an essential aspect of the anti-inflammatory mechanism of IDR-1002 peptide. This highlights the ability of IDR-1002 to differentially modulate the immune response depending on the inflammatory triggers. Furthermore, the pathway mediating the leukocyte extravasation process was among the top pathways downregulated by IDR-1002 treatment (Table II). This included many leukocyte adhesion molecules from the selectin family and the integrin family (Supplemental Fig. 3A). These results supported the observation that IDR-1002 attenuated neutrophil infiltration and effectively dampened PMA-induced ear inflammation.

IRFs constitute a family of transcription factors and play essential roles in host defense and inflammation (72, 73). Irf8 is expressed in macrophages, dendritic cells, and T and B lymphocytes (74, 75). Irf8 was previously shown to be essential in the differentiation and functions of macrophages and dendritic cells, generation of a Th1 response in response to IFN-γ, and protection against intracellular pathogens, including *Mycobacterium tuberculosis*, *Salmonella* Typhimurium, and *Helicobacter pylori* (54, 75–79). In this study, we found that PMA upregulated the expression of seven IRFs (Irf1, Irf4, Irf5, Irf6, Irf7, Irf8, Irf9), and only Irf8 was downregulated when IDR-1002 treatment was provided (Supplemental Fig. 3B). More importantly, comparing combined IDR-1002 and PMA treatment with PMA challenge alone revealed that Irf8 was a major hub in the protein–protein interaction network, interacting with 28 other dysregulated gene products involved in innate and adaptive immunity. Many of these Irf8 interactors play a role in disorders with inflammatory etiology. For example, Irf8 participates in the transcriptional regulation of TLR4 signaling in murine lung during endotoxemia (56). Irf8 and Stat1 have been shown to mediate the cross-talk between LPS-induced TLR4 signaling and the IFN-γ response; both are key processes contributing to the early stages of atherosclerosis and plaque development (48). Furthermore, Irf8-regulated Ccl5, Isg15, Cd274, Oasl2, Slc15a3, and Gbp2 expression was previously found to drive the pathological inflammation during cerebral malaria (80). These results support the possibility that, by suppressing the key transcription factor Irf8, IDR-1002 could potentially control a variety of inflammatory responses mediated by Irf8 target genes, such as Ccl5, TNF-α, and TLR4. Because there is no clinical development of anti-inflammatory agents targeting Irf8 (48), these results also highlight the value of IDR-1002 as a novel therapeutic candidate for combating inflammatory diseases. IDR-1002 can modulate multiple signaling transduction pathways by acting on cell surface receptors, as well as intracellular targets. MAPKs, PI3K, and the NF-κB signaling pathway have all been shown to be essential for IDR-1002 activity (18). A previous study demonstrated that sequestosome-1/p62 is the key intracellular target of IDR-1 (81). IDR-1002 could potentially interact with targets similar to those used by IDR-1 (18). In particular, overexpression of sequestosome-1/p62 has been shown to inhibit Irf8 activities and modulate NF-κB activities, which, in turn, attenuate cytokine gene expression in activated macrophages (82). The detailed mechanism of how IDR-1002 modulates the Irf8-connected network in the context of sterile inflammation is not fully understood and requires future investigation.

Acknowledgments

We thank Reza Falsafi for preparing RNA-Seq libraries, Dr. Mariena J.A. van der Plas for providing the protocol for in vivo ROS imaging, Dr. Hamid Masoudi for quantifying immune cell populations in the H&E-stained specimens, Dr. Erin E. Gill for generating the reads per kilobase of tran-

script per million mapped reads table, and Dr. Evan F. Haney for reading an earlier draft of the manuscript.

Disclosures

Peptide IDR-1002 is the subject of US patent 9707282 granted to R.E.W.H. and three other inventors, assigned to their employer the University of British Columbia, and licensed to ABT Innovations Inc. The other authors have no financial conflicts of interest.

References

1. Medzhitov, R. 2008. Origin and physiological roles of inflammation. *Nature* 454: 428–435.
2. Rock, K. L., E. Latz, F. Ontiveros, and H. Kono. 2010. The sterile inflammatory response. *Annu. Rev. Immunol.* 28: 321–342.
3. Chen, G. Y., and G. Nuñez. 2010. Sterile inflammation: sensing and reacting to damage. *Nat. Rev. Immunol.* 10: 826–837.
4. McDonald, B., K. Pittman, G. B. Menezes, S. A. Hirota, I. Slaba, C. C. Waterhouse, P. L. Beck, D. A. Muruve, and P. Kubes. 2010. Intravascular danger signals guide neutrophils to sites of sterile inflammation. *Science* 330: 362–366.
5. Rider, P., Y. Carmi, O. Guttman, A. Braiman, I. Cohen, E. Voronov, M. R. White, C. A. Dinarello, and R. N. Apte. 2011. IL-1α and IL-1β recruit different myeloid cells and promote different stages of sterile inflammation. *J. Immunol.* 187: 4835–4843.
6. Heneka, M. T., M. J. Carson, J. El Khoury, G. E. Landreth, F. Brosseron, D. L. Feinstein, A. H. Jacobs, T. Wyss-Coray, J. Vitorica, R. M. Ransohoff, et al. 2015. Neuroinflammation in Alzheimer's disease. *Lancet Neurol.* 14: 388–405.
7. Murdoch, J. R., and C. M. Lloyd. 2010. Chronic inflammation and asthma. *Mutat. Res.* 690: 24–39.
8. Tuttolomondo, A., D. Di Raimondo, R. Pecoraro, V. Arnao, A. Pinto, and G. Licata. 2012. Atherosclerosis as an inflammatory disease. *Curr. Pharm. Des.* 18: 4266–4288.
9. Molfino, N. A., and P. K. Jeffery. 2007. Chronic obstructive pulmonary disease: histopathology, inflammation and potential therapies. *Pulm. Pharmacol. Ther.* 20: 462–472.
10. Firestein, G. S. 2003. Evolving concepts of rheumatoid arthritis. *Nature* 423: 356–361.
11. Tabas, I., and C. K. Glass. 2013. Anti-inflammatory therapy in chronic disease: challenges and opportunities. *Science* 339: 166–172.
12. Singh, J. A., K. G. Saag, S. L. Bridges, E. A. Akl, R. R. Bannuru, M. C. Sullivan, E. Vaysbrot, C. McNaughton, M. Osani, R. H. Shmerling, et al. 2016. 2015 American College of Rheumatology guideline for the treatment of rheumatoid arthritis. *Arthritis Rheumatol.* 68: 1–26.
13. Celli, B. R., M. Decramer, J. A. Wedzicha, K. C. Wilson, A. A. Agustí, G. J. Criner, W. MacNee, B. J. Make, S. I. Rennard, R. A. Stockley, et al; ATS/ERS Task Force for COPD Research. 2015. An official American Thoracic Society/European Respiratory Society statement: research questions in COPD. *Eur. Respir. Rev.* 24: 159–172.
14. Choi, K. Y., L. N. Chow, and N. Mookherjee. 2012. Cationic host defence peptides: multifaceted role in immune modulation and inflammation. *J. Innate Immun.* 4: 361–370.
15. Mansour, S. C., O. M. Pena, and R. E. Hancock. 2014. Host defense peptides: front-line immunomodulators. *Trends Immunol.* 35: 443–450.
16. Hilchie, A. L., K. Wuerth, and R. E. Hancock. 2013. Immune modulation by multifaceted cationic host defense (antimicrobial) peptides. *Nat. Chem. Biol.* 9: 761–768.
17. Pena, O. M., N. Afacan, J. Pistolic, C. Chen, L. Madera, R. Falsafi, C. D. Fjell, and R. E. Hancock. 2013. Synthetic cationic peptide IDR-1018 modulates human macrophage differentiation. *PLoS One* 8: e52449.
18. Nijnik, A., L. Madera, S. Ma, M. Waldbrook, M. R. Elliott, D. M. Easton, M. L. Mayer, S. C. Mullaly, J. Kindrachuk, H. Jenssen, and R. E. Hancock. 2010. Synthetic cationic peptide IDR-1002 provides protection against bacterial infections through chemokine induction and enhanced leukocyte recruitment. *J. Immunol.* 184: 2539–2550.
19. Turner-Brannen, E., K. Y. Choi, D. N. Lippert, J. P. Cortens, R. E. Hancock, H. El-Gabalawy, and N. Mookherjee. 2011. Modulation of interleukin-1β-induced inflammatory responses by a synthetic cationic innate defence regulator peptide, IDR-1002, in synovial fibroblasts. *Arthritis Res. Ther.* 13: R129.
20. Huante-Mendoza, A., O. Silva-García, J. Oviedo-Boyso, R. E. Hancock, and V. M. Baizabal-Aguirre. 2016. Peptide IDR-1002 inhibits NF-κB nuclear translocation by inhibition of IκBα degradation and activates p38/ERK1/2-MSK1–dependent CREB phosphorylation in macrophages stimulated with lipopolysaccharide. *Front. Immunol.* 7: 533.
21. Haney, E. F., S. C. Mansour, A. L. Hilchie, C. de la Fuente-Núñez, and R. E. Hancock. 2015. High throughput screening methods for assessing antibiofilm and immunomodulatory activities of synthetic peptides. *Peptides* 71: 276–285.
22. Niyonsaba, F., L. Madera, N. Afacan, K. Okumura, H. Ogawa, and R. E. Hancock. 2013. The innate defense regulator peptides IDR-HH2, IDR-1002, and IDR-1018 modulate human neutrophil functions. *J. Leukoc. Biol.* 94: 159–170.
23. Gábor, M. 2003. Models of acute inflammation in the ear. *Methods Mol. Biol.* 225: 129–137.
24. Stanley, P. L., S. Steiner, M. Havens, and K. M. Tramposch. 1991. Mouse skin inflammation induced by multiple topical applications of 12-O-tetradecanoylphorbol-13-acetate. *Skin Pharmacol.* 4: 262–271.
25. Darveau, R. P., and R. E. Hancock. 1983. Procedure for isolation of bacterial lipopolysaccharides from both smooth and rough *Pseudomonas aeruginosa* and *Salmonella typhimurium* strains. *J. Bacteriol.* 155: 831–838.
26. van der Plas, M. J., R. K. Bhongir, S. Kjellström, H. Siller, G. Kasetty, M. Mörgelin, and A. Schmidtchen. 2016. *Pseudomonas aeruginosa* elastase cleaves a C-terminal peptide from human thrombin that inhibits host inflammatory responses. *Nat. Commun.* 7: 11567.
27. Ewels, P., M. Magnusson, S. Lundin, and M. Käller. 2016. MultiQC: summarize analysis results for multiple tools and samples in a single report. *Bioinformatics* 32: 3047–3048.
28. Aken, B. L., S. Ayling, D. Barrell, L. Clarke, V. Curwen, S. Fairley, J. Fernandez Banet, K. Billis, C. García Girón, T. Hourlier, et al. 2016. The Ensembl gene annotation system. *Database (Oxford)* 2016: baw093.
29. Dobin, A., C. A. Davis, F. Schlesinger, J. Drenkow, C. Zaleski, S. Jha, P. Batut, M. Chaisson, and T. R. Gingeras. 2013. STAR: ultrafast universal RNA-seq aligner. *Bioinformatics* 29: 15–21.
30. Anders, S., P. T. Pyl, and W. Huber. 2015. HTSeq–a Python framework to work with high-throughput sequencing data. *Bioinformatics* 31: 166–169.
31. Love, M. I., W. Huber, and S. Anders. 2014. Moderated estimation of fold change and dispersion for RNA-seq data with DESeq2. *Genome Biol.* 15: 550.
32. Foroushani, A. B., F. S. Brinkman, and D. J. Lynn. 2013. Pathway-GPS and SIGORA: identifying relevant pathways based on the over-representation of their gene-pair signatures. *PeerJ* 1: e229.
33. Xia, J., E. E. Gill, and R. E. Hancock. 2015. NetworkAnalyst for statistical, visual and network-based meta-analysis of gene expression data. *Nat. Protoc.* 10: 823–844.
34. Breuer, K., A. K. Foroushani, M. R. Laird, C. Chen, A. Sribnaia, R. Lo, G. L. Winsor, R. E. Hancock, F. S. Brinkman, and D. J. Lynn. 2013. InnateDB: systems biology of innate immunity and beyond–recent updates and continuing curation. *Nucleic Acids Res.* 41: D1228–D1233.
35. Rutkowski, R., S. A. Pancewicz, K. Rutkowski, and J. Rutkowska. 2007. [Reactive oxygen and nitrogen species in inflammatory process]. *Pol. Merkur. Lekarski.* 23: 131–136.
36. Kielland, A., T. Blom, K. S. Nandakumar, R. Holmdahl, R. Blomhoff, and H. Carlsen. 2009. In vivo imaging of reactive oxygen and nitrogen species in inflammation using the luminescent probe L-012. *Free Radic. Biol. Med.* 47: 760–766.
37. Salinas-Sánchez, D. O., M. Herrera-Ruiz, S. Pérez, E. Jiménez-Ferrer, and A. Zamilpa. 2012. Anti-inflammatory activity of hautriwaic acid isolated from *Dodonaea viscosa* leaves. *Molecules* 17: 4292–4299.
38. Mittal, M., M. R. Siddiqui, K. Tran, S. P. Reddy, and A. B. Malik. 2014. Reactive oxygen species in inflammation and tissue injury. *Antioxid. Redox Signal.* 20: 1126–1167.
39. Xiao, L., Y. Zhang, S. S. Berr, M. D. Chordia, P. Pramoonjago, L. Pu, and D. Pan. 2012. A novel near-infrared fluorescence imaging probe for in vivo neutrophil tracking. *Mol. Imaging* 11: 372–382.
40. Blanchard, C., M. K. Mingler, M. McBride, P. E. Putnam, M. H. Collins, G. Chang, K. Stringer, J. P. Abonia, J. D. Molkentin, and M. E. Rothenberg. 2008. Periostin facilitates eosinophil tissue infiltration in allergic lung and esophageal responses. *Mucosal Immunol.* 1: 289–296.
41. Hsieh, C. Y., C. L. Chen, C. C. Tsai, W. C. Huang, P. C. Tseng, Y. S. Lin, S. H. Chen, T. W. Wong, P. C. Choi, and C. F. Lin. 2012. Inhibiting glycogen synthase kinase-3 decreases 12-O-tetradecanoylphorbol-13-acetate-induced interferon-γ-mediated skin inflammation. *J. Pharmacol. Exp. Ther.* 343: 125–133.
42. Hsieh, C. Y., C. L. Chen, Y. S. Lin, T. M. Yeh, T. T. Tsai, M. Y. Hong, and C. F. Lin. 2014. Macrophage migration inhibitory factor triggers chemotaxis of CD74+CXCR2+ NKT cells in chemically induced IFN-γ-mediated skin inflammation. *J. Immunol.* 193: 3693–3703.
43. Zhang, G., X. Liu, C. Wang, L. Qu, J. Deng, H. Wang, and Z. Qin. 2013. Resolution of PMA-induced skin inflammation involves interaction of IFN-γ and ALOX15. *Mediators Inflamm.* 2013: 930124.
44. Salmela, M., P. Rappu, J. Lilja, H. Niskanen, E. Taipalus, J. Jokinen, and J. Heino. 2016. Tumor promoter PMA enhances kindlin-2 and decreases vimentin recruitment into cell adhesion sites. *Int. J. Biochem. Cell Biol.* 78: 22–30.
45. Widelitz, R. B. 2008. Wnt signaling in skin organogenesis. *Organogenesis* 4: 123–133.
46. Lim, X., and R. Nusse. 2013. Wnt signaling in skin development, homeostasis, and disease. *Cold Spring Harb. Perspect. Biol.* 5: a0008029.
47. Sun, L., and R. D. Ye. 2012. Role of G protein-coupled receptors in inflammation. *Acta Pharmacol. Sin.* 33: 342–350.
48. Chmielewski, S., A. Piaszyk-Borychowska, J. Wesoly, and H. A. Bluyssen. 2016. STAT1 and IRF8 in vascular inflammation and cardiovascular disease: diagnostic and therapeutic potential. *Int. Rev. Immunol.* 35: 434–454.
49. Simon, P. S., S. K. Sharman, C. Lu, D. Yang, A. V. Paschall, S. S. Tulachan, and K. Liu. 2015. The NF-κB p65 and p50 homodimer cooperate with IRF8 to activate iNOS transcription. *BMC Cancer* 15: 770.
50. Kinoshita, T., R. Imamura, H. Kushiyama, and T. Suda. 2015. NLRP3 mediates NF-κB activation and cytokine induction in microbially induced and sterile inflammation. *PLoS One* 10: e0119179.

51. Fritsche, G., M. Nairz, I. Theurl, S. Mair, R. Bellmann-Weiler, H. C. Barton, and G. Weiss. 2007. Modulation of macrophage iron transport by Nramp1 (Slc11a1). *Immunobiology* 212: 751–757.
52. Holmdahl, R., O. Sareila, L. M. Olsson, L. Bäckdahl, and K. Wing. 2016. Ncf1 polymorphism reveals oxidative regulation of autoimmune chronic inflammation. *Immunol. Rev.* 269: 228–247.
53. Hamilton, J. A. 2008. Colony-stimulating factors in inflammation and autoimmunity. *Nat. Rev. Immunol.* 8: 533–544.
54. Alter-Koltunoff, M., S. Goren, J. Nousbeck, C. G. Feng, A. Sher, K. Ozato, A. Azriel, and B. Z. Levi. 2008. Innate immunity to intraphagosomal pathogens is mediated by interferon regulatory factor 8 (IRF-8) that stimulates the expression of macrophage-specific Nramp1 through antagonizing repression by c-Myc. *J. Biol. Chem.* 283: 2724–2733.
55. Liu, J., and X. Ma. 2006. Interferon regulatory factor 8 regulates RANTES gene transcription in cooperation with interferon regulatory factor-1, NF-kappaB, and PU.1. *J. Biol. Chem.* 281: 19188–19195.
56. Pedchenko, T. V., G. Y. Park, M. Joo, T. S. Blackwell, and J. W. Christman. 2005. Inducible binding of PU.1 and interacting proteins to the Toll-like receptor 4 promoter during endotoxemia. *Am. J. Physiol. Lung Cell. Mol. Physiol.* 289: L429–L437.
57. Vila-del Sol, V., C. Punzón, and M. Fresno. 2008. IFN-gamma-induced TNF-alpha expression is regulated by interferon regulatory factors 1 and 8 in mouse macrophages. *J. Immunol.* 181: 4461–4470.
58. Hotamisligil, G. S. 2006. Inflammation and metabolic disorders. *Nature* 444: 860–867.
59. Hancock, R. E., E. F. Haney, and E. E. Gill. 2016. The immunology of host defence peptides: beyond antimicrobial activity. *Nat. Rev. Immunol.* 16: 321–334.
60. Rivas-Santiago, B., J. E. Castañeda-Delgado, C. E. Rivas Santiago, M. Waldbrook, I. González-Curiel, J. C. León-Contreras, J. A. Enciso-Moreno, V. del Villar, J. Mendez-Ramos, R. E. Hancock, and R. Hernandez-Pando. 2013. Ability of innate defence regulator peptides IDR-1002, IDR-HH2 and IDR-1018 to protect against *Mycobacterium tuberculosis* infections in animal models. *PLoS One* 8: e59119.
61. Boardman, P. L., and F. D. Hart. 1967. Side-effects of indomethacin. *Ann. Rheum. Dis.* 26: 127–132.
62. Lövgren, O., and E. Allander. 1964. Side-effects of indomethacin. *BMJ* 1: 118.
63. Naito, Y., T. Yoshikawa, N. Yoshida, and M. Kondo. 1998. Role of oxygen radical and lipid peroxidation in indomethacin-induced gastric mucosal injury. *Dig. Dis. Sci.* 43(9 Suppl.): 30S–34S.
64. Niyonsaba, F., A. Someya, M. Hirata, H. Ogawa, and I. Nagaoka. 2001. Evaluation of the effects of peptide antibiotics human beta-defensins-1/-2 and LL-37 on histamine release and prostaglandin D(2) production from mast cells. *Eur. J. Immunol.* 31: 1066–1075.
65. Dinarello, C. A. 2011. Interleukin-1 in the pathogenesis and treatment of inflammatory diseases. *Blood* 117: 3720–3732.
66. Turner, M. D., B. Nedjai, T. Hurst, and D. J. Pennington. 2014. Cytokines and chemokines: at the crossroads of cell signalling and inflammatory disease. *Biochim. Biophys. Acta* 1843: 2563–2582.
67. Bradley, J. R. 2008. TNF-mediated inflammatory disease. *J. Pathol.* 214: 149–160.
68. Pollard, K. M., D. M. Cauvi, C. B. Toomey, K. V. Morris, and D. H. Kono. 2013. Interferon-γ and systemic autoimmunity. *Discov. Med.* 16: 123–131.
69. Shen, H., D. Kreisel, and D. R. Goldstein. 2013. Processes of sterile inflammation. *J. Immunol.* 191: 2857–2863.
70. Bralley, E. E., J. L. Hargrove, P. Greenspan, and D. K. Hartle. 2007. Topical anti-inflammatory activities of *Vitis rotundifolia* (muscadine grape) extracts in the tetradecanoylphorbol acetate model of ear inflammation. *J. Med. Food* 10: 636–642.
71. Calou, I. B., D. I. Sousa, G. M. Cunha, G. A. Brito, E. R. Silveira, V. S. Rao, and F. A. Santos. 2008. Topically applied diterpenoids from *Egletes viscosa* (Asteraceae) attenuate the dermal inflammation in mouse ear induced by tetradecanoylphorbol 13-acetate- and oxazolone. *Biol. Pharm. Bull.* 31: 1511–1516.
72. Ozato, K., P. Tailor, and T. Kubota. 2007. The interferon regulatory factor family in host defense: mechanism of action. *J. Biol. Chem.* 282: 20065–20069.
73. Taniguchi, T., K. Ogasawara, A. Takaoka, and N. Tanaka. 2001. IRF family of transcription factors as regulators of host defense. *Annu. Rev. Immunol.* 19: 623–655.
74. Wang, H., and H. C. Morse, III.. 2009. IRF8 regulates myeloid and B lymphoid lineage diversification. *Immunol. Res.* 43: 109–117.
75. Marquis, J. F., O. Kapoustina, D. Langlais, R. Ruddy, C. R. Dufour, B. H. Kim, J. D. MacMicking, V. Giguère, and P. Gros. 2011. Interferon regulatory factor 8 regulates pathways for antigen presentation in myeloid cells and during tuberculosis. *PLoS Genet.* 7: e1002097.
76. Tamura, T., T. Nagamura-Inoue, Z. Shmeltzer, T. Kuwata, and K. Ozato. 2000. ICSBP directs bipotential myeloid progenitor cells to differentiate into mature macrophages. *Immunity* 13: 155–165.
77. Tamura, T., P. Thotakura, T. S. Tanaka, M. S. Ko, and K. Ozato. 2005. Identification of target genes and a unique *cis* element regulated by IRF-8 in developing macrophages. *Blood* 106: 1938–1947.
78. Xiong, H., H. Li, H. J. Kong, Y. Chen, J. Zhao, S. Xiong, B. Huang, H. Gu, L. Mayer, K. Ozato, and J. C. Unkeless. 2005. Ubiquitin-dependent degradation of interferon regulatory factor-8 mediated by Cbl down-regulates interleukin-12 expression. *J. Biol. Chem.* 280: 23531–23539.
79. Yan, M., H. Wang, J. Sun, W. Liao, P. Li, Y. Zhu, C. Xu, J. Joo, Y. Sun, S. Abbasi, et al. 2016. Cutting edge: expression of IRF8 in gastric epithelial cells confers protective innate immunity against *Helicobacter pylori* infection. *J. Immunol.* 196: 1999–2003.
80. Berghout, J., D. Langlais, I. Radovanovic, M. Tam, J. D. MacMicking, M. M. Stevenson, and P. Gros. 2013. Irf8-regulated genomic responses drive pathological inflammation during cerebral malaria [Published erratum appears in 2015 *PLoS Pathog.* 11: e1004719.]. *PLoS Pathog.* 9: e1003491.
81. Yu, H. B., A. Kielczewska, A. Rozek, S. Takenaka, Y. Li, L. Thorson, R. E. Hancock, M. M. Guarna, J. R. North, L. J. Foster, et al. 2009. Sequestosome-1/p62 is the key intracellular target of innate defense regulator peptide. *J. Biol. Chem.* 284: 36007–36011.
82. Kim, J. Y., and K. Ozato. 2009. The sequestosome 1/p62 attenuates cytokine gene expression in activated macrophages by inhibiting IFN regulatory factor 8 and TNF receptor-associated factor 6/NF-κB activity. *J. Immunol.* 182: 2131–2140.